High resolution lake sediment record reveals self-organized criticality in erosion processes regulated by internal feedbacks

Running title: Drivers of erosion variability estimated by a high-resolution record

D. Colombaroli [1,2]*, D.G. Gavin[3*], A.E. Morey[4], V.R. Thorndycraft[1]

1. Centre for Quaternary Research, Department of Geography, Royal Holloway, University of London, Egham, Surrey, TW200EX
2. University of Bern and Oeschger Centre for Climate Change Research, Bern, Switzerland
3. Department of Geography, University of Oregon, Eugene OR 97403-1251
4. College of Earth, Ocean, and Atmospheric Sciences, Oregon State University, Corvallis, OR 97331-5503

* Both authors contributed equally to this manuscript.

Corresponding Author: Daniele Colombaroli (daniele.colombaroli@rhul.ac.uk)

This article has been accepted for publication and undergone full peer review but has not been through the copyediting, typesetting, pagination and proofreading process which may lead to differences between this version and the Version of Record. Please cite this article as doi: 10.1002/esp.4383

Abstract

Reconstruction of high-frequency erosion variability beyond the instrumental record requires well-dated, high-resolution proxies from sediment archives. We used computed tomography (CT) scans of finely laminated silt layers from a lake-sediment record in southwest Oregon to quantify the magnitude of natural landscape erosion events over the last 2000 years in order to compare with palaeorecords of climate, forest fire, and seismic triggers. Sedimentation rates were modeled from an age-depth relationship fit through five ^{14}C dates and the 1964 AD ^{137}Cs peak in which deposition time (yr mm^{-1}) varied inversely with the proportion of silt sediment measured by the CT profile. This model resulted in pseudo-annual estimates of silt deposition for the last 2000 years. Silt accumulation during the past 80 years was strongly correlated with river-discharge at annual and decadal scales, revealing that erosion was highly responsive to precipitation during the logging era (1930–present). Prior to logging the frequency-magnitude relationship displayed a power-law distribution that is characteristic of complex feedbacks and self-regulating mechanisms. The 100-year and 10-year erosion magnitude estimated in a 99-year moving window varied by 1.7 and 1.0 orders of magnitude, respectively. Decadal erosion magnitude was only moderately positively correlated with a summer temperature reconstruction over the period 900–1900 AD. Magnitude of the seven largest events were similar to the cumulative silt accumulation anomaly, suggesting these events “returned the system” to the long-term mean rate. Instead, the occurrence of most erosion events was related to fire (silt layers preceded by high charcoal concentration) and earthquakes (the seven thickest layers often match paleo-earthquake dates). Our data show how internal (i.e., sediment production) and external processes (natural fires or more stochastic events such as earthquakes) co-determine erosion regimes at millennial time scales, and the extent to which such processes can be offset by recent large-scale deforestation by logging.

Keywords (5): computed tomography, hill-slope erosion, fire, logging, self-regulating systems.

1. Introduction

High rainfall events are the primary source of sediment runoff from hillslopes into upland streams and lakes (Zolitschka, 1998; Lamoureux, 2002; Glur et al., 2013; Swierczynski et al., 2013), Forecasted increases in the frequency of heavy precipitation (Sillmann et al., 2013) may cause important shifts in hydrological and geomorphic processes, but the significance of such changes for catchment erosion processes are difficult to assess on the basis of short-term instrumental observations. Lake sediment archives can be used to extend the record of individual sediment flux events through the reconstruction of event stratigraphies (Thorndycraft et al., 1998), which, in records that span millennia, can be used to infer magnitude and frequency relationships of rainfall/flood events (e.g. Czymzyk et al., 2010; Glur et al., 2013; Swiercynski et al., 2013). High resolution lake-derived erosion histories often indicate centennial to millennial scale climate variability may exert a first-order control over the magnitude of erosion rates (Lamoureux, 2002; Meyer and Pierce, 2003; Pierce et al., 2004:, Schillereff et al, 2016). However, whilst lake sediment records provide important data on magnitude and frequency of individual sediment delivery events triggered by rainfall (Glur et al., 2013; Swiercynski et al., 2013; Schillereff et al., 2016), the relationship between erosion events and climate can be difficult to disentangle because sediment delivery may be mediated by other landscape scale processes (e.g. fires or earthquakes), which can overprint (or even offset) the climatic control over erosion dynamics (Fig. 1). Furthermore, internal system dynamics may play an important modulating role on sediment processes and subsequently on the sediment archive. Model simulations, for example, have shown that identical floods can generate different bedload sediment yields demonstrating

self-organised criticality and suggesting sediment archives may not record external drivers (Van De Wiel and Coulthard, 2010).

To investigate these themes high resolution records of multiple drivers are required that enable the role of different controls to be deciphered. Catchments influenced by both wildfires and tectonics can provide such an opportunity as proxy datasets such as charcoal concentration and earthquake generated turbidites may allow insights into causation of sediment delivery events. Upper Squaw Lake in the Siskiyou region of Oregon and California provides an excellent case study to investigate such controls on catchment erosion because the charcoal record shows that fires of both low and high severity have been a key driver for vegetation structure and composition over millennia, affecting slope stability and therefore post-fire erosion events (Colombaroli and Gavin 2010). Additionally, the availability of regional Late Holocene records for earthquake events (Morey-Ross, 2013), Pacific Northwest summer temperature (Mann et al., 2008), and regional winter precipitation and temperature (Ersek et al., 2012), allow direct comparison between multiple external controls. Furthermore, the onset of logging in the catchment over recent decades, which increased sediment fluxes (Colombaroli and Gavin, 2010; Richardson et al., in press), enables a comparison of natural versus anthropogenic controls on sediment flux.

The main aim of the paper, therefore, is to investigate the roles of climate, fire and earthquakes on catchment erosion, during natural state and post-logging conditions. We applied a novel computed tomography (CT) approach on a lake sediment core from Upper Squaw Lake to model sedimentation rates at a sufficiently high temporal resolution (annual to multiannual) to achieve this aim. Furthermore, using the CT-derived silt-inwash record we test whether the frequency and

magnitude of erosion events follow a power-law distribution, indicative of an ordered "self-organized" system (Bak et al., 1988), with erosion controlled by the balance between internal variability and local (e.g. fire) to regional scale (climatic) processes. We hypothesise erosion to be mostly driven by climatic extremes (i.e. precipitation) during the logging period (A.D. 1950), as road construction and the removal of trees decreased soil resilience to weathering. In contrast, prior to logging, erosion events may increase with precipitation (i.e., floods), earthquakes, or the disturbance regimes in the catchment.

2. Material and methods

2.1 Setting

Upper Squaw Lake (42° 2' N; 123° 0.9′ W; 930 m a.s.l.) is a landslide-dammed basin in the Applegate valley, draining ca. 40 km² of upstream watershed within 1000 m of relief (Fig. 2). Steep topography of the watershed and schist bedrock makes this site particularly responsive to erosion, with the lake acting as a trap for sediment pulses. Minerogenic material can enter directly in the upper lake via slopewash or by suspended load from Squaw Creek, deposited in the deepest part of the lake from suspension. The relatively flat bottom of the lake indicates that sub-aqueous landslides or slumping of lake floor sediments were likely not important at the core site (Supplementary S1). The 10-m, 2000-year record was previously studied for vegetation and high-resolution fire history, though inferences regarding erosion were limited by a 1-cm sampling resolution (Colombaroli and Gavin, 2010).

Sediment is mobilized during extreme rainfall events (e.g. as in 1997), which in this area are the result of the dominant south-westerly flow of moisture-laden air associated with the Aleutian Low during the winter months (80% of the ca. 1100 mm

annual mean occurs from November to April). However, the largest precipitation events are associated with “atmospheric rivers:” long bands of water vapor from lower latitudes in the Pacific Ocean (Gimeno et al., 2014). Snowmelt floods transporting finer terrigenous layers (Lamoureux and England, 2000) may also occur when a warm air mass causes rain-on-snow in the upper elevations of the watershed. Summer months are warm and dry, and streamflow into the lake in late summer is negligible.

Flood-transported minerogenic sediments require a supply of sediment that is generated by weathering and punctuated by mass movements. Landsliding is common in the Condrey Mountain schist in the watershed (Fig. 2); such landslides may be associated with extreme precipitation, though a previous study matched some of the larger events in the core with earthquake events identified at the coast (Morey et al., 2013). Forest fires are also common within the watershed; Colombaroli and Gavin (2010) noted that many silt layers followed charcoal peaks suggesting a major role of fire in controlling forest dynamic over centuries, and amplifying the effect of hydrology on erosion.

2.2 Computed tomography CT scans of lake-sediment radiodensity

Using the sediment core from Upper Squaw Lake previously studied by Colombaroli and Gavin (2010), we obtained CT scans of radiodensity (expressed as Hounsfield Units, HU) using a Toshiba Aquilion 64-Slice at the Oregon State University College of Veterinary Medicine. Longitudinal cross section images of each core were selected using OSIRI-X software, and values from overlapping 1-m core drives were correlated and aligned to match sampling depths used in Colombaroli and Gavin (2010). HU values were then averaged at each depth along a ca. 5-mm wide

transect, avoiding voids in the sediment, using open source ImageJ software (http://rsbweb.nih.gov/ij/). The resulting series of 23,016 values had a median resolution of 0.46 mm, but ranged from 0.2 to 0.6 mm among images. We therefore binned the series to a constant 1-mm interval by integrating values across the irregular sampling resolution.

2.3 Estimation of annual time series of accumulated silt

We used a Bayesian-like approach to develop a sediment chronology that accounts for the rapid deposition of erosion layers as estimated by the high-resolution CT measurements, following Colombaroli and Gavin (2010) and Kelly et al. (2013). We assume sediment is a mixture of nearly-instantaneous deposited silt and slowly deposited organic matter. This method calculates the proportion of silt (θ) in each mm depth, by scaling radiodensity (Hounsfield units; HU) as: $(\rho_d-\rho_{min})/(\rho_{crit}-\rho_{min})$, where ρ_d is the radiodensity at depth d, ρ_{min} is the minimum radiodensity observed (200 HU in this study), and ρ_{crit} is the critical radiodensity (ca. 753 HU, see below). Core segments above the ρ_{crit} threshold are considered instantaneous and therefore θ is set to 1 (100% silt). We calculated the effective depth (ED_d) as the depth after removing the silt component as estimated by θ. The critical density ρ_{crit} was estimated as the value that minimized the root-mean-square-error (RMSE) of a linear regression between ED_d and seven age-control points (five radiocarbon dates, one Cs-137 profile, and the core top; Colombaroli and Gavin, 2010). Ages were assigned to the effective depths by fitting a monotonic spline between the effective depths and the age estimates, thus accounting for naturally varying rates of sedimentation that are common in sediment cores (Kelly et al., 2013). This model was performed on 1000 resamples of the calibrated radiocarbon probability distributions to obtain the

median and 90th percentile confidence envelope for ages at each effective depth, resulting in a strong fit (RMSE=97±32 years among simulations) and agreement with ρ_{crit} (median=753 HU, 5th to 95th percentiles are 715 and 784 HU, respectively). The resampling of radiocarbon dates resulted in a distribution of ages at each 1-mm depth; the 5th, 50th, and 95th percentiles of ages were retained. We then integrated the θ values from the depth scale within intervals corresponding to annual increments, which resulted in estimates of pseudo-annual values of silt deposition (E, mm/yr). Separate time series of E were developed for the 5th, 50th, and 95th percentiles of age estimates for each depth.

To assess the extent to which silt deposition is driven by storm-related erosion events, we compared the last 150 years of E to a composite record of peak annual discharge from the region. Annual data from five stream gages on the Applegate, Rogue, and Klamath Rivers were standardized relative to the Copper gage on the Applegate River and then averaged for the period with at least three gages reporting (1939–2007).

2.4 Erosion frequency-magnitude relationship

From the annual time series, we examined the frequency-magnitude relationship of annual silt accumulation (E) vs return period, to assess the peak-magnitude distribution and the occurrence of anomalously large, low-frequency events (Kidson and Richards, 2005). We applied reduced major axis (RMA) regression (Legendre and Legendre, 1988) to obtain linear fits of the log-log relationship between magnitude and recurrence interval (lmodel2 package for R statistical software). Two lines were fit: the first was fit to the portion of the plot between return periods of ca. 1.5 and 100 years; the second was fit between return periods of 10 and 100 years.

We chose these values because 1) the left side of the plot was curvi-linear and several authors (Kidson and Richards, 2005; Malamud and Turcotte, 2006) suggest simply censoring such data, and 2) we wished to examine whether these lines extrapolated to the magnitude of the largest, most infrequent, events (>100 year recurrence intervals).

We used two methods to assess the stationarity of the frequency-magnitude relationship. First, we used RMA regression as described above in a moving 99-year window. From the fitted line, we estimated the 2-year, 10-year, and 100-year events (E_2, E_{10}, and E_{100}, respectively), with their 95% confidence envelopes. Second, we calculated E_2, E_{10}, and E_{100} directly from the data using running quantiles (Koenker and Bassett, 1978) in a 99-year moving window. The 100th (maximum), 90.91th, and 50.5th quantiles correspond to E_{100}, E_{10}, and E_2, respectively. These time series were then smoothed using a loess smoother within a 99-year window.

To assess the importance of the largest events on the overall sedimentation rates, we plotted the cumulative departure from the mean rate of silt deposition of the pre-logging period (Lamoureux, 2002). Additional plots were constructed after substituting the seven largest events (> 75 mm) and the 64 largest events (> 10 mm) with the mean of the remaining values. To assess whether the magnitude of the seven largest events were related to cumulative departure from the mean rate (i.e., whether these events “returned the system” to the mean rate), we calculated the standard deviation of the cumulative departures following the seven largest events. This value was compared to 1000 Monte Carlo simulations of the same standard deviation statistic in which, for each simulation, the seven large events were inserted into the record on randomly chosen years.

2.5 Potential drivers of erosion: fire, climate, and earthquakes

We assessed the link between fire and erosion by compositing the charcoal concentration data from the same core (quantified at the 1-cm scale with a 2-yr mean resolution; Colombaroli and Gavin 2010) in the 20 years leading and lagging major silt events. Separate analyses were run for the largest seven silt events (>75 mm) and the 57 next-largest events (10 – 75 mm). Significant departures of the composited charcoal concentrations from the mean was assessed from the 95% confidence interval generated from 10,000 resamplings (of randomly chosen years) of the full charcoal record.

To compare erosion history with climate proxies with similar temporal resolution in the region, we explored several high-resolution reconstructions from the Pacific Northwest, including a multi-proxy reconstruction of summer temperature (Mann et al., 2008) and stable isotope records from speleothems at Oregon Caves National Monument (Ersek et al., 2012), located 30 km west of Upper Squaw Lake, which are sensitive to winter precipitation ($\delta^{13}C$) and winter temperature ($\delta^{18}O$). We focused these comparisons on the smoothed E_2 and E_{10} reconstructions, as they are less sensitive to single large events but still captures the pattern of erosion intensity through time. Few other climate proxies are suitable for contrasting with USL, as they are either too distant (Steinman et al., 2012) or with too poor absolute chronology to compare to USL (Pyramid Lake, NV; Benson et al. 2002).

Last, the possibility that the largest events were triggered by earthquakes was considered by comparing the largest erosion events with reconstructed seismic records from the Cascadia subduction zone. The age-probability distribution of the seven largest silt events was calculated from resampling of radiocarbon dates in the construction of the age model (see above). These distributions were plotted against

the age estimates of tsunamis at Bradley Lake, Oregon (Kelsey et al., 2005) and age estimates of off-shore turbidites (Goldfinger et al., 2012).

3. Results

3.1 Sediment chronology and erosion history

The 10-m core (ca. 2,000 years, Fig. 3) consists of organic lake mud (gyttja) alternating with coarser, terrigenous layers of varying thickness (Fig. 3 a,b). Density of sediment measured by CT provides a high-resolution proxy for deposition of allochthonous mineral matter. CT values were linearly related to measured bulk density (r^2=0.92, n=61 samples) and negatively related with the percentage of organic matter estimated by loss-on-ignition (r^2=0.84; S2). Biogenic silica was only ca. 15% of the sediment dry weight with no down-core trend (Colombaroli and Gavin, 2010).

Our Bayesian-like approach for estimating chronology (Fig. 3c), which collapsed silt layers into instantaneous events, resulted in an almost linear accumulation rate (S3). The lower and upper probabilities (calculated on resampled dates), have higher age uncertainties in the lower part of the sequence (±200 yrs in 200 AD) than higher in the sequence (±100 yrs in 800 AD) due to larger ^{14}C errors (Colombaroli and Gavin, 2010). The high-resolution (at the 1-mm scale) variation in sedimentation density resulted in a time series of silt events at annual resolution, with almost all years represented by at least 1 mm of sediment. Silt deposition accounted for ca. 75% of the total accumulated sediment and silt layers greater than a few mm in thickness had a fining-upward structure (seen by highest CT values capping the layer, S5) suggesting that they are single events rather than multiple events straddling more than one year. The seven largest events preceding 1930 AD

(at 200, 630, 1005, 1250, 1375, 1705, and 1920 AD) represent ca. 30% of the silt accumulation for that period. The top ca. 3 m of homogeneous inorganic material was deposited in four large events after logging and road building started in the catchment (AD 1950). The age model indicates that of the 7.46 m of silt deposited over the 2000-year record, 3.01 m (40%) occurred after initial road construction in ca. 1930 AD, indicating an 11.5-fold increase in sedimentation from the previous mean rate.

The peaks in silt accumulation over the last 150 years follows the history of peak annual streamflow (Fig. 4). The five largest floods (AD 1965, 1997, 1956, 1974, and 2006) are close in time to some of the largest reconstructed erosion events (AD 1965, 2007, 1961, 1975, and 1954) suggesting sensitivity of our site location to the magnitude of recurrent floods (e.g Schillereff et al., 2016). Earlier historic floods pre-dating the gage-station record (in AD 1861, 1890, and 1927) are close in time to other reconstructed erosion events, especially considering dating uncertainties (Fig. 4). Furthermore, the decadal-scale variation in peak discharge mirrors the decadal-scale variation in silt accumulation, with high values in the 1950's to 1970's declining to lower values thereafter.

3.2 Erosion frequency-magnitude relationship

The frequency-magnitude relationship of CT-inferred depositional thickness for the period before logging generally shows a power-law distribution (Fig. 5). Events with a 10, 100, and 1000-year return periods were of magnitudes of 3.5, 22.8, and 207.0 mm, respectively. On the left side of this relationship the frequency-magnitude relationship was not linear but rather the magnitude of events with intervals less than 1.5 years were increasingly of lower magnitude than expected from the remainder of

the data. The RMA regression fit to events with a 1.5 to 100-year return period (Fig. 5, green line, slope=0.97) over-predicts the magnitude of events with intervals greater than ca. 75 years. In contrast, the RMA regression fit to only events with a 10 to 100-year return period (Fig. 5, orange line, slope=0.82) follows the data closely within the interval range of 10 to 250 years, but when extrapolating it underpredicts the observed magnitude of the most infrequent events (>250 year intervals), and overpredicts the magnitude of the most frequent events (<10 year intervals).

Calculated in a 99-year moving window, the magnitude of the 100-year event (E_{100}) varies 1.5 orders of magnitude prior to AD 1930 due to the occurrence of seven thick layers (Fig. 6). E_{100} shows a quasi-periodic trend over the last 2000 years (every ca. 400 yrs, with E_{100} peaks around 200, 600, 1000, 1300, 1700 AD). Estimates of E_{100} in a 99-year moving window differed whether using the fitted values from RMA regression (yellow solid line and confidence interval in Fig. 6) versus the observed value from smoothed quantiles (yellow dashed line in Fig. 6). This difference is the result of an underestimate of the RMA to the largest events in the frequency-magnitude distribution in the 99-year moving window, confirming that the underestimation of the largest events in the overall plot (Fig. 5) also holds for frequency-magnitude relationships limited to the century surrounding the large events. Similar centennial-scale variations are also shown (but to a lesser extent) by the E_{10} and E_2 estimates. The estimated values (from the fits of the RMA regression) of E_{10} and E_{100} (expressed as log values) are strongly correlated over time (r=0.93), but the observed values (from smoothed quantiles) are much less so (r=0.47) indicating a non-stationary frequency-magnitude relationship. Correlation of E_2 and E_{10} over time are also moderate (r=0.79 and 0.83 for the regression estimate and quantiles, respectively).

Estimated sediment accumulation departure from mean rate over the last 2000 years (Fig. 6b) shows nearly constant deposition over the centennial scale, only interrupted markedly by the seven largest-magnitude events. Furthermore, the magnitude of these seven events was related to the amount the accumulated sediment diverged from the mean rate. The standard deviation of the values of the accumulated sediment anomaly after the seven largest events (circles in Fig 6b) was significantly smaller than would be expected if these events were randomly placed in time (P=0.03; S4). This suggests the magnitude of the largest events was dependent on the time elapsed since the previous large event, "returning the system" to its long-term mean. Removing the largest events from the record shows greatly reduced variation in the sediment accumulation departures (dashed and thin red lines in Fig. 6c) and that the period before ca. 1600 AD had generally higher-than-average rates while lower-than-average rates occurred after 1600 AD until the logging era, at which time sediment accumulation increases abruptly.

3.3 Potential drivers of erosion: fire, climate, and earthquakes

The seven largest silt events are preceded by, on average, a five-fold increase of charcoal concentration (Fig. 7). This pattern was statistically significant for the 1–3 years preceding the silt event. Examining the patterns of charcoal and silt concentration on a depth scale shows a repeated pattern of a simultaneous and abrupt increase in charcoal and sediment density (i.e. silt concentration), after which charcoal concentrations decrease after ca. 3 cm but sediment density continues to increase for many more cm, consistent with a fining-upward pattern resulting from settling of the suspended sediment load (S5), and likely subsequent remobilization and sediment focusing. The 57 smaller silt events (10-75 mm in magnitude) are

preceded by an almost doubling of charcoal concentration, which was statistically significant from six years before to two years after the silt event (Fig. 7 and S5). This suggests that smaller fires or fires preceding flood events by more than three years resulted in smaller erosion events. In addition, erosion magnitude was generally higher during decadal-to-centennial scale episodes of fire events as previously reconstructed from the same sediment record (Colombaroli and Gavin, 2010; S6).

Comparison of the erosion record with regional proxies of paleoclimate resulted in weak correspondence between climate and erosion magnitude (Fig. 8). We focused on comparing E_{10} and E_2 with paleoclimate proxies, as these quantiles are not driven by singular large events. E_{10} generally matches centennial-scale variability of July temperature as reconstructed for the Pacific Northwest region (Mann et al., 2009), with episodes of higher erosion occurring during warm periods of the Medieval Climatic Anomaly (1000-1400 AD) but less so during the Little Ice Age (1450-1850 AD). An isotope record from speleothems at Oregon Caves National Monument shows pronounced variability in winter-season rainfall (recorded in $\delta^{13}C$) and winter temperature (recorded in $\delta^{18}O$). Most periods of increased erosion occur during drier (higher $\delta^{13}C$) and cooler winter (lower $\delta^{18}O$) periods.

The seven largest erosion events have a moderate match with reconstructed earthquake and tsunami events. However, the correlation is limited by the chronological control in the first half of our record (S7).

4. Discussion

4.1 Logging impacts on catchment erosion

Hundreds of minerogenic layers in the Upper Squaw Lake (USL) core show the occurrence of high-frequency, low-magnitude erosion events over the last 2000

years, whilst individual thicker silt deposits record low frequency erosion events of higher magnitude. When summarized in a moving 99-year window the erosion history is marked by rapid changes in erosion magnitude and frequency. This history is likely the result of complex interactions between regional climate, disturbance processes and other more stochastic events (such as earthquakes). When identified in the paleorecord, the different drivers of erosion variability may help explain highly non-stationary erosion processes (E_2, E_{10} and E_{100}) as evidenced by our record (Fig. 6).

Within the chronological uncertainties of the two records, flood deposits generally occur during historic floods (Fig. 4), showing that terrigenous in-wash layers can be associated to storm-related floods of different magnitude (e.g. Noren et al., 2002). This relationship between erosion and floods is particularly marked following logging within the USL watershed (i.e., events between 1950 to 1965 AD, 1996 and after 2000 AD), showing how road building for logging can greatly amplify erosion during high rainfall events (Fig. 4 and Colombaroli and Gavin 2010). Indeed, the four erosion events following road construction were on average 2.4 times greater than the largest four events of the last 2000 years, and the mean sedimentation rate increased 11-fold following logging. The highly erodible schist bedrock combined with sidecasting of soils during road construction provided abundant sediment input to streams, thereby increasing sediment flux, and lake sediment accumulation rate (Fig. 3), beyond pre-disturbance rates.

4.2 Frequency-magnitude relationship in erosion events

Prior to disturbance by logging and roadbuilding, the distribution of the estimated annual thicknesses of silt deposition follows a frequency-magnitude relationship (log-

log plot in Fig. 5) that is indicative of a power law (rather than normal) distribution (Kidson and Richards, 2005). This suggests a scaleless, structured hierarchy of sediment-layer magnitude.

The linear frequency-magnitude relationship is particularly apparent for return periods of 10 to 100 years (orange line in Fig. 5). The power exponent of this relationship (0.82) is similar to the exponent of flood magnitude for a similar-sized watershed in California (0.90; Malamud and Turcotte, 2006), which would be expected if there was a correlation between hydrologic variability and erosion variability.

The observed frequency-magnitude relationship diverges from the linear fit when extrapolating outside of the 10–100 years interval period. The magnitude of the events with short return periods (<2 years) are distinctly smaller than that expected from a linear relationship. This feature is common in frequency-magnitude relationships of annual peak stream discharge (Kidson and Richards, 2005). A potential solution proposed for discharge data is to use a “partial duration series” on sub-annual data (which often resolves this downturn on the left side of the plot; Fig. 5). Such an approach is not possible with our data because our reconstructed events likely integrate over at least one year. Another cause of this downturn is that the sediment record may simply not detect the smallest events. There may be a threshold level of sediment load and stream discharge that transports suspended minerogenic sediments to the core site, which lies more than 100 m from the delta, and therefore the smallest events may be largely undetected in our record.

The extrapolation of the frequency-magnitude relationship to longer intervals shows an underprediction of the observed magnitude of the largest events. The RMA regression line follows the data closely up to 250-year intervals, at which point six of

the seven largest events have a magnitude of at least 50 mm greater than that expected from the linear relationship. These large events also drove a non-stationary pattern in the frequency-magnitude relationship.

Calculated in a moving 99-year window, the estimates of the 2-year, 10-year, and 100-year events varied markedly, by up to 1.7 orders of magnitude. Overall, the frequency-magnitude distribution may results from the sum of exponentials of multiple processes (Ramsay, 2006). In our case this include both internal (e.g., sediment storage within the stream network) and external processes (regional climate, fire disturbances and other more stochastic events such as earthquakes), though mechanisms underlying the largest events deserve special attention.

4.3 Local scale processes constraining soil production and erosion.

When summarized in a moving 99-year window (Fig. 6) the erosion record at USL is marked by rapid shifts in sediment accumulation rates. At the multi-decadal scale, soil erosion is limited by on-site soil availability, which depends on local soil productivity and consequent accumulation (e.g. Heimsath et al., 1997).

Slow accumulation of terrigenous material in the USL record can be visualized using the cumulative sediment departure curve, showing periods with constant and lower rates accumulation punctuated by rapid erosion events (Fig 6). Continuous sediment accumulation is likely a precondition for high-magnitude erosion events to occur, as repeated events tend to reduce soil stocks (e.g. Smith et al., 2001), and make the system less prone to erosion following storm events (e.g. Page et al., 1994). At our site, the cumulative amount of silt deposition following the seven major events is significantly closer to the mean rate than the value calculated by a randomization test (Fig. S4), showing that event magnitude is related to the time

elapsed since the last large event. For example, one of the largest events recorded in our lake (1000 AD) occurred after several centuries of slow sediment accumulation, suggesting that high magnitude events may require a sufficient amount of sediment accumulated in the stream system (Turcotte et al., 1999). The intervals between these large events is not constant over time, but rather short or long periods result in varying magnitude of erosion events, indicating the role of other processes in mediating sediment erosion (see above). The relative dependence of large events with the time since last disturbances suggests a memory of the system for the erosion budget (Lamoureux, 2002). Removal of sediment by these large events results in a much more stationary pattern of cumulative sediment accumulation (Fig. 6b). The millennial-scale trend in these cumulative series indicates that even smaller events contribute to the long-term changes in sediment accumulation.

Together, these results suggest a significant role of accumulation and storage of sediments in the stream network which are then discharged during a small number of extreme events (Lamoureux and England, 2000, Glur et al., 2013). Lamoureux (2002) invoked similar processes to explain an annual series of sedimentation in a lake in the Canadian arctic in which E_{10}-magnitude events were preceded by lower-than-average sedimentation, though the E_{100}-magnitude events were preceded by an increase in sedimentation. Lamoureux (2002) suggested this was a sign of increased sediment loads that led to a triggering of a hysteresis in which a major sediment delivery occurred during the next runoff event. We did not detect any such lead and lag effects around the large sedimentation rates at USL (analyses not shown). Rather, we suggest external triggering mechanisms

(discussed below) were critical at USL for determining the timing of the major events, in contrast to an internal-to-the-watershed hysteresis process.

4.4 Climatic versus non-climatic controls of erosion magnitude

Soil sensitivity to erosion depends on many factors including slope exposure (e.g. Roering, 2008), vegetation cover, logging, stand replacing fires or triggered by large events such as earthquakes (Montgomery and Brandon, 2002; Dadson et al., 2004; Pierce et al., 2004; Valentin et al., 2005, Richardson et al., in press). When identified in the paleorecord, the different drivers of erosion variability may help explain the erosion time series (E_2, E_{10} and E_{100}), evidenced by our record (Fig. 6). Indeed, the largest events in the USL record are not predicted by the power law frequency-magnitude relationship; rather, they seem to be exceptional in the context of the last 2000 years of erosion variability (Fig. 5). These events cause the estimate of E_{100} to vary by 1.7 orders of magnitude over the last 2000 years (Fig. 5). Below, we assess the drivers for major erosion events with a focus on fire variability, given that our record provide data to quantify disturbance regime interaction (i.e. fire vs. erosion) at a greater resolution.

Particularly severe, stand-replacing fire events are a main driver of vegetation changes in the mixed conifer forest of the Siskyou Mountains, as shown by pollen and lake-sediment charcoal from the same record (Colombaroli and Gavin, 2010). In particular, paleoecological evidences show how a mixed-severity fire regime largely determined the marked changes in vegetation composition and structure, with relatively fast recovery of ponderosa pine or Douglas-fir following disturbances at a timescale of few decades at most (Colombaroli and Gavin 2010 and Fig. 1). Severe and stand replacing fires also play an important role in removing vegetation and

destabilizing soils by removal of the O horizon, reducing infiltration capacity, and promoting water repellency that increase rill erosion (e.g. Certini, 2005; Shakesby and Doerr, 2006, Orem and Pelletier, 2015). Heat from fire can drive water-repellent compounds deeper into the soil thus creating a sheer layer at depth which can cause larger slides and debris flows. On steep slopes in the watershed, we noted several old, inactive, debris-flow channels that may be a legacy of such debris flows following past fires.

Erosion events identified by the CT-scan data closely follow episodes of increased charcoal deposition in the lake (Fig. S-5). The time series analyses show that the largest events lagged only 1–3 years after high charcoal concentrations (Fig. 7), with erosion continuing after charcoal peaks already decreased, at least in few large events (S5). In contrast, the smaller erosion events were preceded by six years of moderately high charcoal concentration, though not close to the magnitude for the largest events. This may have been due to less severe fires or a delay between the year of the fire and the year of erosion, such that vegetation re-establishment of early successional and riparian trees (e.g. ponderosa pine and alder, Fig.1 and Colombaroli & Gavin 2010) reduced the erosion amount. The charcoal sampling resolution (1-cm sampling intervals) is too coarse to infer the role of high frequency fires and thinner silt layers. For example, some erosion events seem not to be directly preceded by fire (Fig. S-5). Overall, our data reveal the extent to which fire mediated the erosion process.

Summer droughts or exceptionally dry winters are the major drivers of fire variability in the region at the seasonal to the millennial scales (Agee, 1993). The regional paleoclimate record (Mann et al., 2009) shows periods of warmer temperature, such as during the MCA (950-1250), and cold conditions during the

Little Ice Age (1400-1700 AD) resulting in changing fire frequency over time (Colombaroli and Gavin 2010). In addition, the Oregon Cave stable isotope record suggests a pronounced variability in winter-season rainfall (recorded in $\delta^{13}C$) and winter temperature (recorded in $\delta^{18}O$). The close link between fires in the watershed and a tree-ring reconstruction of summer drought in the area (Cook et al., 2004) again highlights how climate has been an important determinant of fire occurrence in our area (Colombaroli and Gavin, 2010).

In contrast, the relationship between erosion and climate is less straightforward than with fire, suggesting that climate variability may not be the dominant factor of erosion variability (Fig 8). Within the age uncertainties of independently dated records, erosion variability seems to be enhanced during periods of warmer temperature, such as during the MCA (950-1250), and reduced during cold conditions (Little Ice Age: 1400-1700 AD, Mann et al., 2009). Higher erosion during warmer periods may simply reflect increased fire occurrence during warmer and drier periods (see above), although the length of the Mann (2009) reconstruction precludes assessing the temperature control on large events before 500 AD. The comparison with the Oregon Cave stable isotope record show that erosion peaks generally occurred under both drier (higher $\delta^{13}C$) and cooler winters (lower $\delta^{18}O$). Dry winter conditions in the Pacific Northwest are also often cold due to blocking of warm-wet onshore flow; these conditions result in decreased snowpack and increased fire hazard (Westerling et al., 2006). In addition, colder winters would maintain deeper snowpack longer in the season at this mid-elevation location, which then may contribute to spring floods.

This relative low sensitivity of erosion to changing climate at our site suggests the importance of stand scale processes at landscape scale and/or self-organised

criticality in system behaviour (e.g. Van De Wiel and Coulthard, 2010). Additionally, the position of our site relative to the north-south dipole pattern of precipitation (Dettinger et al., 1998; Wise, 2010), may also highlight a weaker, or less predictable, response to the centennial scale climate variability, again underlying that in our region more local processes may be the primary driver of erosion variability. Regionally-dependent differences in the sensitivity and response of erosion to specific climate patterns have been also observed for the Alps (Wilhelm et al. 2013; Glur et al. 2013, Wirth et al. 2013).

Earthquakes are another potential trigger for erosion events detected in the USL core (Fig. 1). Earthquakes have been invoked to explain existence of "homogenites" in lake sediments (e.g., Page et al., 1994) and form thick-graded deposit layers that are indicative of rapid deposition (Morey et al., 2013). Within the age uncertainties of both seismogenic turbidities recorded offshore and our record (Goldfinger et al., 2012), it remains difficult to accurately match the historical earthquakes recorded near the coast of the California/Oregon border to specific erosion events in USL (Fig.S-7, and Morey et al., 2013), and therefore the attribution of each drivers (earthquakes, fire, but also extreme floods and other disturbance regimes) remains elusive at this step. Nevertheless, our cumulative departure (Fig. 6) suggest that negative feedbacks (governed by in situ soil production) are important constraints for the quasi-periodic occurrence of large events at the multi-decadal to centennial scale.

5. Conclusions

Our data are indicative of non-stationary frequency-magnitude relationship in erosion regime over millennia, with a historical variability greater than has been estimated

from monitoring and even other paleo-flood studies (Meyer et al., 1992; Zolitschka, 1998; Lamoureux, 2002; Meyer and Pierce, 2003; Pierce et al., 2004). Heterogeneous distributions (power-law) are often considered the result of an ordered behavior, which is not primarily controlled by top-down (climate) processes, but depends upon an internal variability in which the self-organization to a “critical state” (Bak et al., 1988) comes from collective interactions of processes. At our site, erosion variability is mostly constrained by negative feedbacks on-site (i.e. soil production), and indicates how a tradeoff exists between internal and externally (climate) driven erosion processes, thus highlighting the importance of self-regulating mechanisms for sediment runoff in the watershed (Van De Wiel and Coulthard 2010). This ability of mechanisms that can “self-regulate” are likely highly landscape dependent, and vary greatly across landscapes. In this sense, frequency-area distributions for specific landscapes may allow calculating magnitude of erosion events at specific frequencies and could be extended to a full range of ecosystem disturbances, including fire and insect outbreaks. Ecosystem specific relationship can be potentially used for risk assessment of big events (Malamud and Turcotte, 2006). Also, when applied to paleorecords, changes in the frequency/magnitude relationship may be indicative of major landscape reorganization following e.g. cultural transitions (e.g. during the Neolithic in the Alps and southern Europe, Colombaroli et al., 2008, 2013), underlying the relevance of past anthropogenic factors in determining current landscape and disturbance regime conditions.

6. Acknowledgements

The study was supported by Swiss National Foundation Fellowship PBBEA 117553 (to D.C.), with additional support to D.G.G. from the University of Oregon and to A.E.M. from Oregon State University.

The authors declare no conflict of interest.

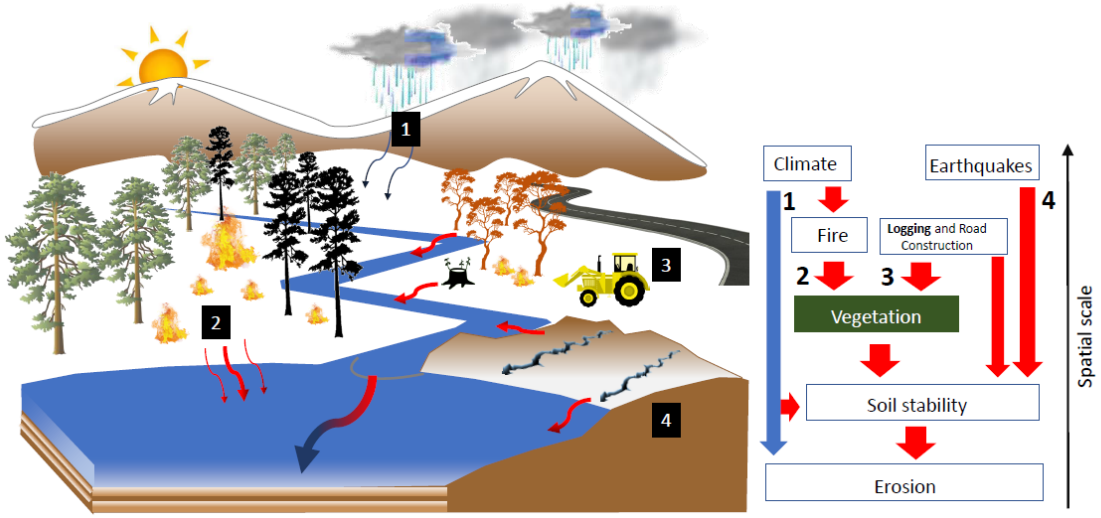

Fig 1. Conceptual figure illustrating the main processes controlling erosion regimes (left), and scales at which they may interact in our catchment (right). Blue arrows indicate the top-down control on erosion and red arrows show the indirect processes which may offset the climate-erosion relationship; both may contribute to sedimentation in the lake (red-blue arrow). The key role of vegetation, a major controller of slope stability and soil development rates (Heimsath et al., 1997), is highlighted by its central position in the diagram (right panel). 1) Climate (e.g. precipitation) controls on erosion. 2) A mixed fire regime (a combination of fires of different intensities) occurred over the last millennia in forest characterized by ponderosa pine (black) and Douglas-fir (dark green) over the last millennia (Colombaroli and Gavin 2010). 3) Runoff further increased in the last decades (thick red arrows), as a consequence of logging, road construction and fires, promoting more disturbance adapted species like the Pacific madrone (*Arbutus menziesii*, dark orange). 4) Large, infrequent earthquakes can further decrease slope stability, increasing erosion rates in the rivers and the lake. Climate also indirectly controls soil stability and erosion after logging events (red arrow); other drivers of runoff at landscape scale such as hillslope and sediment storage in river systems are not shown.

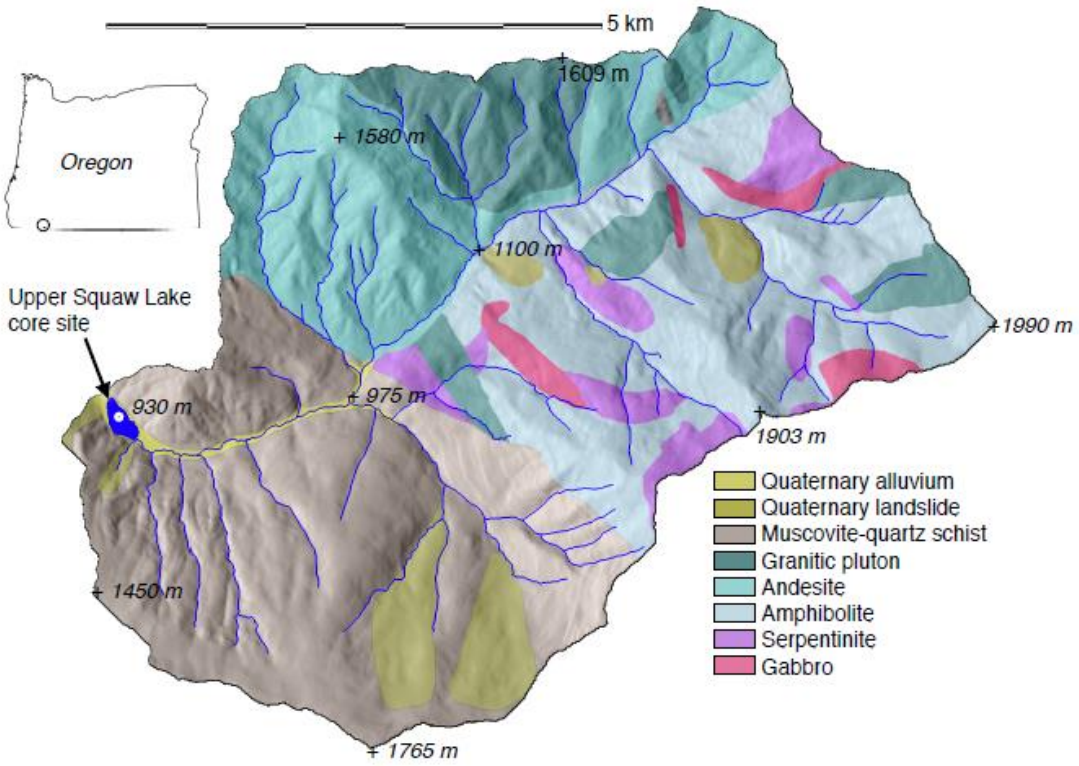

Fig. 2 Geologic map of the 40 km^2 watershed of Upper Squaw Lake located in the southwestern Oregon; modified from Donato, 1993.

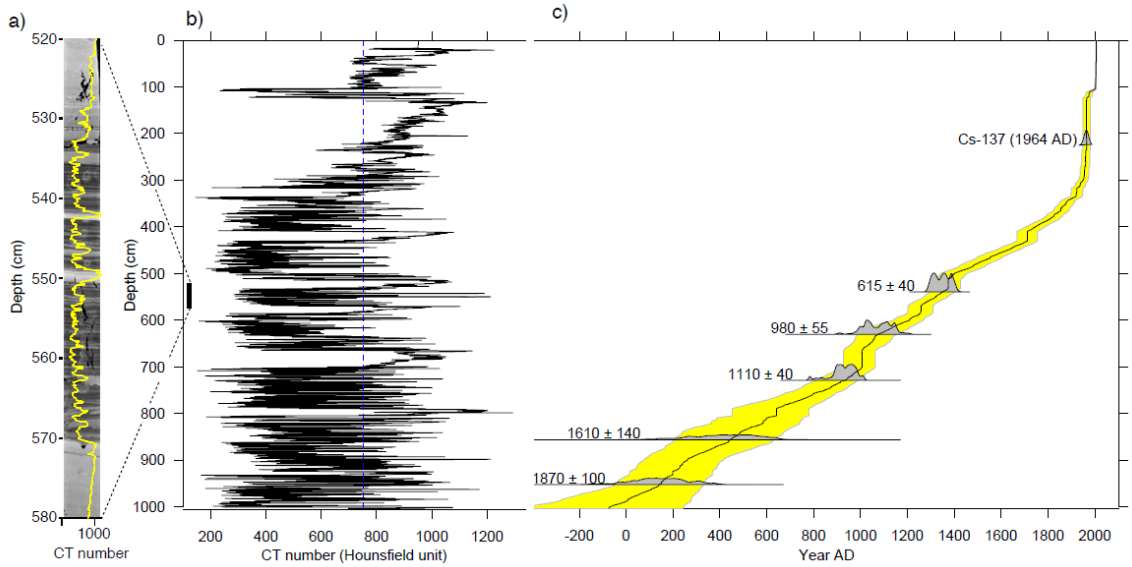

Fig. 3. a) An example of a CT image from the USL core showing alternation of dark gyttja and light clay layers associated with sediment runoff from the watershed and higher HU values. The extracted values are shown as an overlaid yellow line; b) the series of CT values integrated to 1 mm intervals for the 10m core; c) the depth–age model estimated from age control points (core top and Cs and ^{14}C dates) and the CT values (see methods).

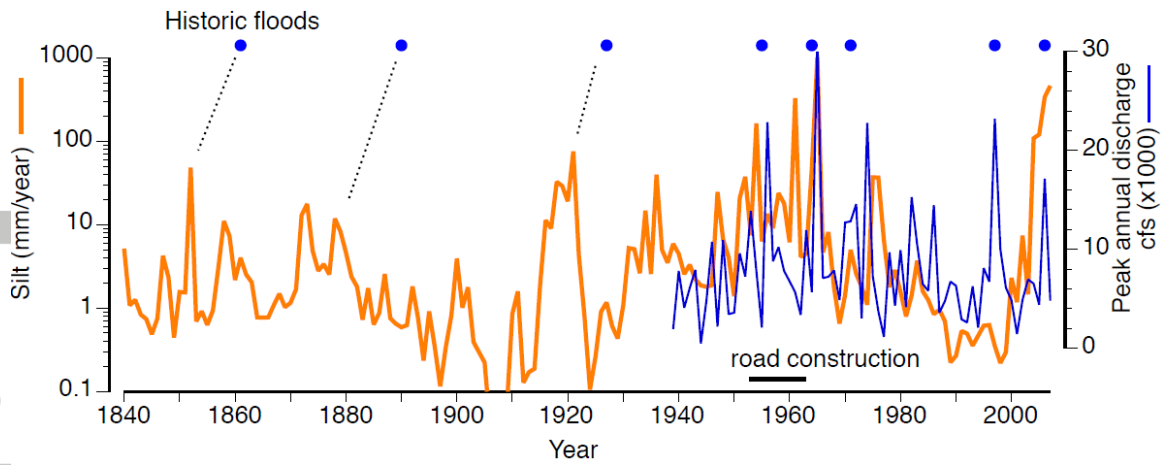

Fig. 4. Inferred annual silt accumulation (thick line) plotted with average annual peak discharge for five regional gage stations, standardized to the Applegate Copper gage. The largest eight historic floods on the Rogue and Klamath rivers since 1860 are indicated as points above the graph. Dashed lines are potential matches of historic floods with peaks in silt accumulation.

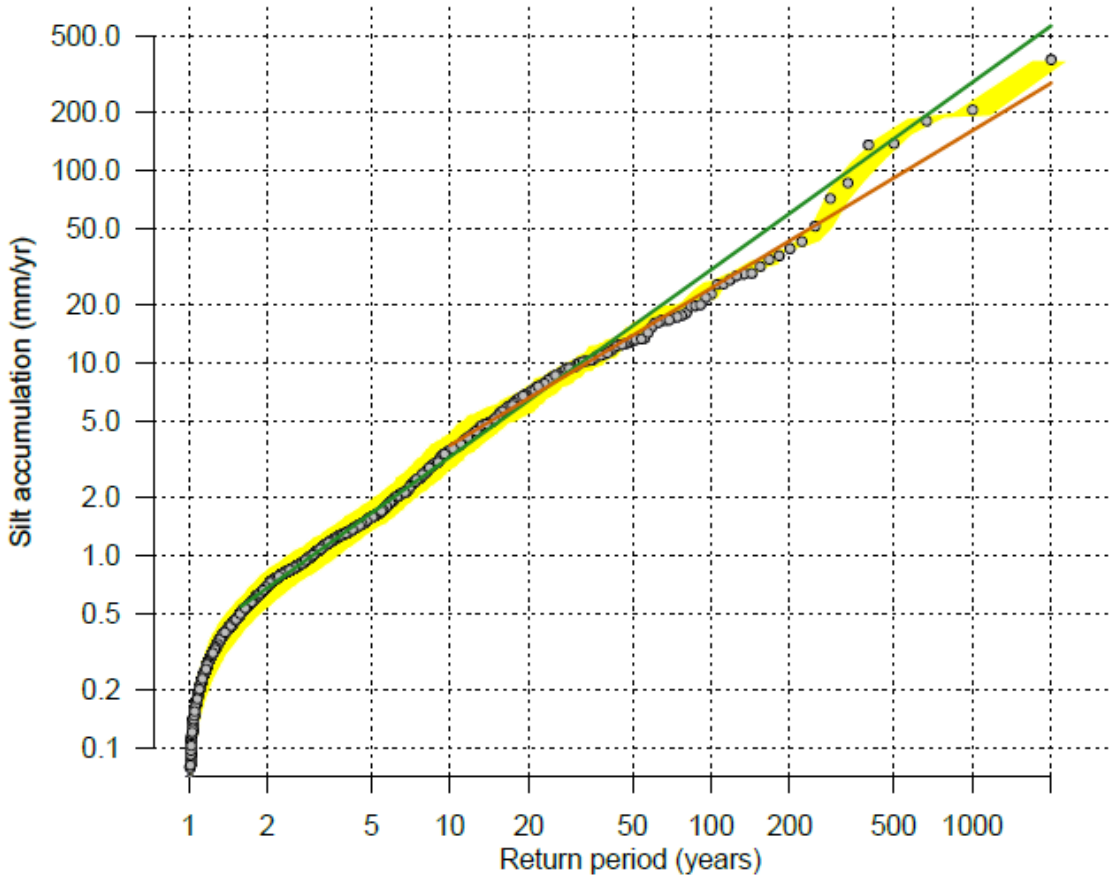

Fig. 5. The relationship between frequency and magnitude of erosion events for the period before AD 1930 inferred from the USL core. Yellow background indicates the range of plotted points that could occur if using different age models (Fig. 3). The green line was fit to events > 0.5 mm in magnitude and 1.5-100 years return periods while the orange line was fit only to events with return periods of 10 to 100 years. Extrapolating these lines shows that the seven largest events depart from the power-law relationship.

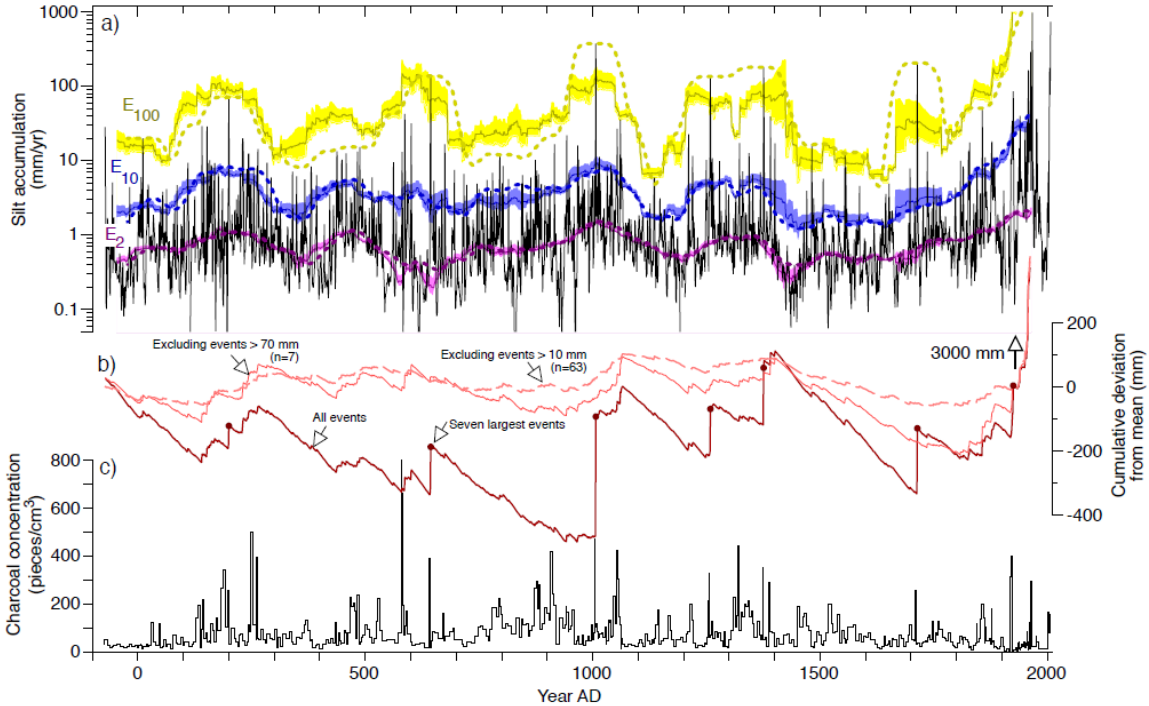

Fig. 6. a) Pseudo-annual silt accumulation plotted on a log scale showing estimates of the 100-year (yellow), 10-year (blue), and 2-year (purple) return-interval event magnitudes (E_{100}, E_{10}, and E_2, respectively) calculated in a 99-year moving window. Solid line and background shading indicate the estimated values and 95% confidence intervals from RMA regression. Thin dashed lines are loess-smoothed quantiles within the same moving window; b) cumulative deviation of sediment accumulation from the mean for the period before AD 1930. Lines were also calculated after removing the seven largest events and the 64 largest events with the mean values. Positive excursions occur at erosion events and descending trends correspond to the slow accumulation of sediment between events; c) charcoal concentration showing distinct peaks resulting from fire (Colombaroli and Gavin 2010).

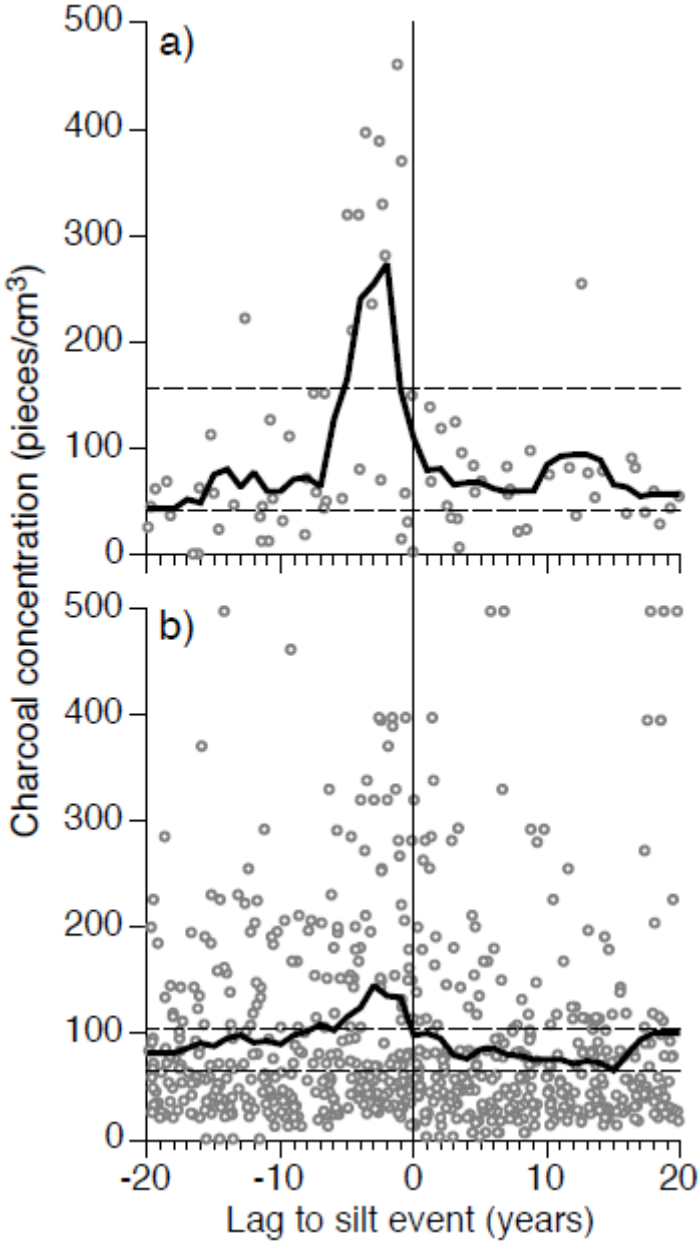

Fig. 7. Composited charcoal concentration values preceding and following silt events for a) the seven largest silt events (>75 mm) preceding AD 1930, and b) the 57 next-largest events (10 – 75 mm). The solid lines are a moving 7-point or 57-point average for a and b, respectively. The dashed lines are 95% confidence intervals generated from 10,000 resamples of the charcoal data set (Fig. 6c).

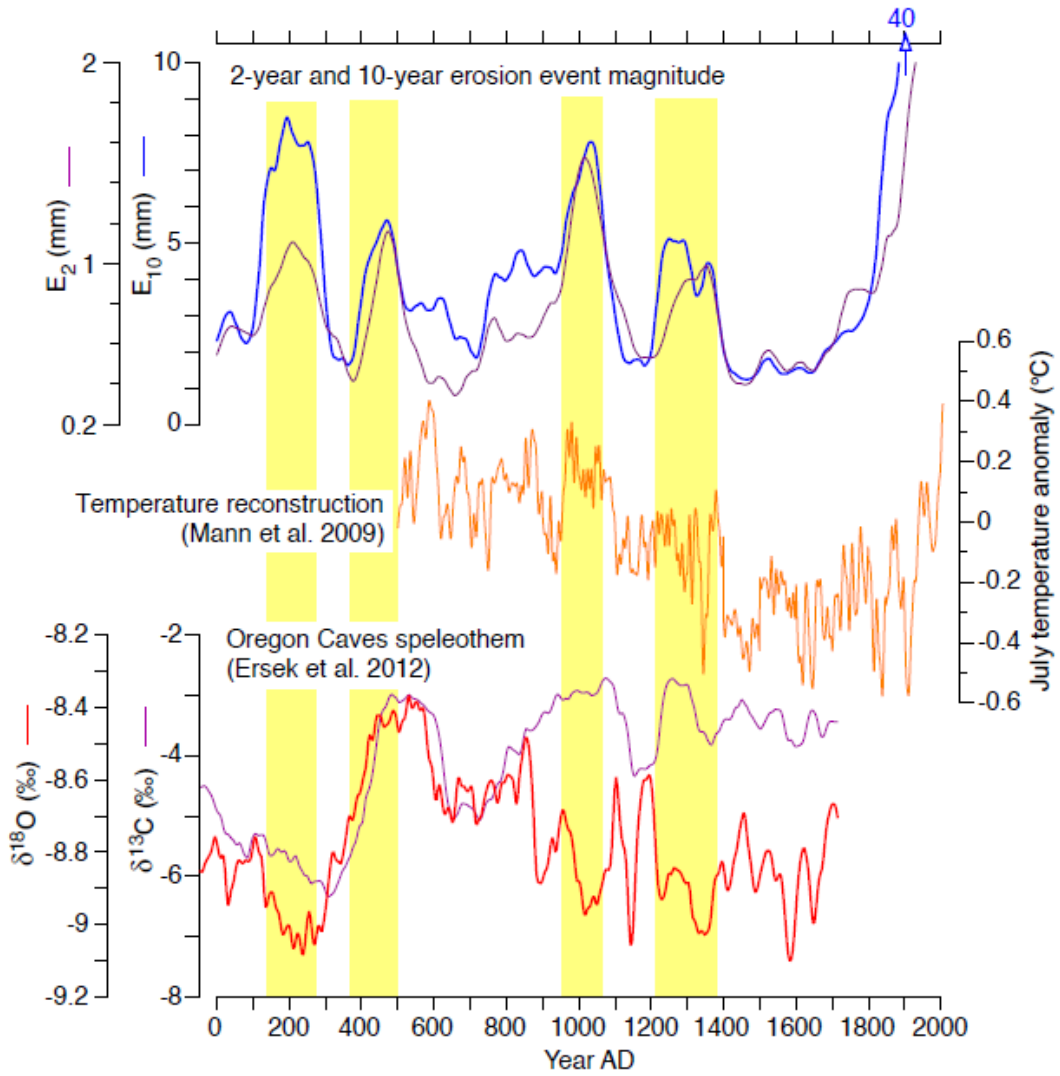

Fig. 8. The magnitude of the 2-year and 10-year erosion event (E_2 and E_{10}) in a moving 99-year window calculating using a loess smoother (from Fig. 6a) compared with a temperature reconstruction for the Pacific Northwest (Mann et al. 2009) and isotope records from Oregon Caves (Ersek et al., 2012). Yellow bars indicate periods of increased erosion magnitude prior to logging road construction.

References

Agee JK. 1993. Fire Ecology of Pacific Northwest Forests. Island Press, Washington DC, 493 pp.

Amann B, Szidat S, Grosjean M. 2015. A millennial-long record of warm season precipitation and flood frequency for the North-western Alps inferred from varved lake sediments: implications for the future. Quaternary Science Reviews 115:89-100.

Bak P, Tang C, Wiesenfeld K. 1988. Self-organized criticality. Physical Review A 38:364-374.

Benson L, Kashgarian M, Rye R, Lund S, Paillet F, Smoot J, Kester C, Mensing S, Meko D, Lindström S. 2002. Holocene multidecadal and multicentennial droughts affecting Northern California and Nevada. Quaternary Science Reviews 21: 659–682.

Castello AF, Shelton ML. 2004. Winter precipitation on the US Pacific Coast and El Nino Southern oscillation events. International Journal of Climatology 24:481-497.

Certini G. 2005. Effects of fire on properties of forest soils: a review. Oecologia 143:1-10.

Colombaroli D, Gavin DG. 2010. Highly episodic fire and erosion regime over the past 2,000 y in the Siskiyou Mountains, Oregon. Proceedings of the National Academy of Sciences of the United States of America 107:18909-18914.

Colombaroli D, Vanniere B, Emmanuel C, Magny M, Tinner W. 2008. Fire-vegetation interactions during the Mesolithic-Neolithic transition at Lago dell'Accesa, Tuscany, Italy. Holocene 18:679-692.

Colombaroli D, Beckmann M, van der Knaap WO, Curdy P, Tinner W. 2013. Changes in biodiversity and vegetation composition in the central Swiss Alps during the transition from pristine forest to first farming. Diversity and distributions 19(2):157-170.

Cook ER, Woodhouse CA, Eakin CM, Meko DM, Stahle DW. 2004. Long-term aridity changes in the western United States. Science 306:1015-1018.

Czymzik M, Dulski P, Plessen B, von Grafenstein U, Naumann R, Brauer A. 2010. A 450 year record of spring-summer flood layers in annually laminated sediments from Lake Ammersee (southern Germany). Water Resources Research 46, W11528.

Dadson SJ, Hovius N, Chen H, Dade WB, Lin JC, Hsu ML, Lin CW, Horng MJ, Chen TC, Milliman J, Stark CP. 2004. Earthquake-triggered increase in sediment delivery from an active mountain belt. Geology 32:733-736.

Dettinger MD, Cayan DR, Diaz HF, Meko DM. 1998. North-south precipitation patterns in western North America on interannual-to-decadal timescales. Journal of Climate 11:3095-3111.

Donato MM. 1993. Preliminary geologic map of the Squaw Lakes quadrangle, Oregon and California. In: Report UO-F, Editor. pp 93-703.

Ersek V, Clark PU, Mix AC, Cheng H, Edwards RL. 2012. Holocene winter climate variability in mid-latitude western North America. Nature Communications 3.

Gimeno L, Nieto R, Vázquez M, Lavers DA. 2014. Atmospheric rivers: a mini-review. Frontiers in Earth Science: 753.

Glur L, Wirth SB, Buentgen U, Gilli A, Haug GH, Schaer C, Beer J, Anselmetti FS. 2013. Frequent floods in the European Alps coincide with cooler periods of the past 2500 years. Scientific Reports 3.

Goldfinger C, Nelson CH, Morey A, Johnson JE, Gracia E, Enkin R, Dallimore A, Dunhill G, Vallier T. 2012. Turbidite Event History: Methods and Implications for Holocene Paleoseismicity of the Cascadia Subduction Zone, Reston, VA, U.S. In: Geological Survey, USGS Professional Paper 1661-F, 362. p 184.

Heimsath AM, Dietrich WE, Nishiizumi K, Finkel RC. 1997. The soil production function and landscape equilibrium. Nature 388:358-361.

Kelly R, Chipman ML, Higuera PE, Stefanova I, Brubaker LB, Hu FS. 2013. Recent burning of boreal forests exceeds fire regime limits of the past 10,000 years. Proceedings of the National Academy of Sciences of the United States of America 110:13055-13060.

Kelsey HM, Nelson AR, Hemphill-Haley E, Witter RC. 2005. Tsunami history of an Oregon coastal lake reveals a 4600 yr record of great earthquakes on the Cascadia subduction zone. Geological Society of America Bulletin 117:1009-1032.

Kidson R, Richards KS. 2005. Flood frequency analysis: assumptions and alternatives. Progress in Physical Geography 29:392-410.

Koenker R, Bassett G. 1978. Regression quantiles. Econometrica 46:33-50.

Lamoureux S. 2002. Temporal patterns of suspended sediment yield following moderate to extreme hydrological events recorded in varved lacustrine sediments. Earth Surface Processes and Landforms 27:1107-1124.

Lamoureux SF, England JH. 2000. Late Wisconsinan glaciation of the central sector of the Canadian high arctic. Quaternary Research 54:181-188.

Legendre P, Legendre L. 1988. Numerical ecology In: Developments in Environmental Modelling. Amsterdam: Elsevier.

Malamud BD, Turcotte DL. 2006. The applicability of power-law frequency statistics to floods. Journal of Hydrology 322:168-180.

Mann ME, Zhang Z, Hughes MK, Bradley RS, Miller SK, Rutherford S, Ni F. 2008. Proxy-based reconstructions of hemispheric and global surface temperature variations over the past two millennia. Proceedings of the National Academy of Sciences of the United States of America 105:13252-13257.

Mann ME, Zhang ZH, Rutherford S, Bradley RS, Hughes MK, Shindell D, Ammann C, Faluvegi G, Ni FB. 2009. Global Signatures and Dynamical Origins of the Little Ice Age and Medieval Climate Anomaly. Science 326:1256-1260.

Mantua NJ, Hare SR, Zhang Y, Wallace JM, Francis RC. 1997. A Pacific interdecadal climate oscillation with impacts on salmon production. Bulletin of the American Meteorological Society 78:1069-1079.

Meyer GA, Pierce JL. 2003. Climatic controls on fire-induced sediment pulses in Yellowstone National Park and central Idaho: a long-term perspective. Forest Ecology and Management 178:89-104.

Meyer GA, Wells SG, Balling RC, Jull AJT. 1992. Response of alluvial systems to fire and climate change in yellowstone-national-park. Nature 357:147-150.

Montgomery DR, Brandon MT. 2002. Topographic controls on erosion rates in tectonically active mountain ranges. Earth and Planetary Science Letters 201:481-489.

Morey AE, Goldfinger C, Briles CE, Gavin DG, Colombaroli D, Kusler JE. 2013. Are great Cascadia earthquakes recorded in the sedimentary records from small forearc lakes? Natural Hazards and Earth System Sciences 13:2441-2463.

Noren AJ, Bierman PR, Steig EJ, Lini A, Southon J. 2002. Millennial-scale storminess variability in the northeastern United States during the Holocene epoch. Nature 419:821-824.

Orem CA, Pelletier JD. 2015. Quantifying the time scale of elevated geomorphic response following wildfires using multi-temporal LiDAR data: An example from the Las Conchas fire, Jemez Mountains, New Mexico. Geomorphology. 232: 224-238.

Page MJ, Trustrum NA, Dymond JR. 1994. Sediment budget to assess the geomorphic effect of a cyclonic storm, new-zealand. Geomorphology 9:169-188.

Pierce JL, Meyer GA, Jull AJT. 2004. Fire-induced erosion and millennialscale climate change in northern ponderosa pine forests. Nature 432:87-90.

Ramsay CM. 2006. The distribution of sums of certain IID pareto variates. Communications in Statistics-Theory and Methods 35:395-405.

Richardson, K. n. d., J. a. Hatten, and R. a. Wheatcroft. (in press). 1500-years of lake sedimentation due to fire, earthquakes, floods and land clearance in the Oregon Coast Range: Geomorphic sensitivity to floods during timber harvest period. Earth Surface Processes and Landforms.

Roering JJ. 2008. How well can hillslope evolution models "explain" topography? Simulating soil transport and production with high-resolution topographic data. Geological Society of America Bulletin 120:1248-1262.

Shakesby RA, Doerr SH. 2006. Wildfire as a hydrological and geomorphological agent. Earth-Science Reviews 74:269-307.

Schillereff DN, Chiverrell RC, Macdonald N, Hooke JN. 2016. Hydrological thresholds and basin control over paleoflood records in lakes.Geology: 44 (1): 43-46.

Sillmann J, Kharin VV, Zwiers FW, Zhang X, Bronaugh D. 2013. Climate extremes indices in the CMIP5 multimodel ensemble: Part 2. Future climate projections. Journal of Geophysical Research-Atmospheres 118:2473-2493.

Smith SV, Renwick WH, Buddemeier RW, Crossland CJ. 2001. Budgets of soil erosion and deposition for sediments and sedimentary organic carbon across the conterminous United States. Global Biogeochemical Cycles 15:697-707.

Steinman BA, Abbott MB, Mann ME, Stansell ND, Finney BP. 2012. 1,500 year quantitative reconstruction of winter precipitation in the Pacific Northwest. Proceedings of the National Academy of Sciences of the United States of America 109:11619-11623.

Swierczynski T, Lauterbach S, Dulski P, Delgado JM, Merz B, Brauer A. 2013. Mid- to late Holocene flood frequency changes in the northeastern Alps as recorded in varved sediments of Lake Mondsee (Upper Austria). Quaternary Science Reviews, 80, 78-90.

Thorndycraft V, Hu Y, Oldfield F, Crooks PRJ, Appleby PG. 1998. Individual flood events detected in the recent sediments of the Petit Lac d'Annecy, eastern France. The Holocene 8:741–746.

Turcotte D, Malamud BD, Morein G, Newman WI. 1999. An inverse-cascade model for self-organized critical behavior. Physica A 268:629-643.

Valentin C, Poesen J, Li Y. 2005. Gully erosion: Impacts, factors and control. Catena 63:132-153.

Van De Wiel MJ, Coulthard TJ. 2010. Self-organized criticality in river basins: Challenging sedimentary records of environmental change. Geology 38 (1): 87-90.

Westerling AL, Hidalgo HG, Cayan DR, Swetnam TW. 2006. Warming and earlier spring increase western US forest wildfire activity. Science 313:940–943.

Wilhelm B, Arnaud F, Sabatier P, Magand O, Chapron E, Courp T, Tachikawa K, Fanget B, Malet E, Pignol C, Bard E, Dalannoy JJ. 2013. Palaeoflood activity and climate change over the last 1400 years recorded by lake sediments in the north-west European Alps. Journal of Quaternary Science: 28 (2): 189-199.

Wirth SB, Gilli A, Simonneau,A, Ariztegui D, Vannière B, Glur L, Chapron E, Magny M, Anselmetti FS. 2013. A 2000-year long seasonal record of floods in the southern European Alps. Geophysical Research Letters: 40 (15) 4025–4029.

Wise EK. 2010. Spatiotemporal variability of the precipitation dipole transition zone in the western United States. Geophysical Research Letters 37.

Zolitschka B. 1998. A 14,000 year sediment yield record from western Germany based on annually laminated lake sediments. Geomorphology 22:1-17.

High resolution lake sediment reveals self-organized criticality in erosion processes regulated by internal feedbacks

D. Colombaroli [1,2]*, D.G. Gavin[3*], A.E. Morey[4], V.R. Thorndycraft[1]

1. Centre for Quaternary Research, Department of Geography, Royal Holloway, University of London, Egham, Surrey, TW200EX
2. University of Bern and Oeschger Centre for Climate Change Research, Bern, Switzerland
3. Department of Geography, University of Oregon, Eugene OR 97403-1251
4. College of Earth, Ocean, and Atmospheric Sciences, Oregon State University, Corvallis, OR 97331-5503

* Both authors contributed equally to this manuscript.

Highlights:

We used computed tomography (CT) scans from a lake-sediment record in southern Oregon to reconstruct pseudo-annual estimates of silt deposition for the last 2000 years, and the relationship with climate, wildfires, and seismic triggers. The frequency-magnitude relationship displayed a power-law distribution that is characteristic of complex feedbacks and self-regulating mechanisms. Our data show how internal (sediment production) and external (natural fires or earthquakes) co-determined erosion over millennia, and the extent to which it is offset by logging in recent times.

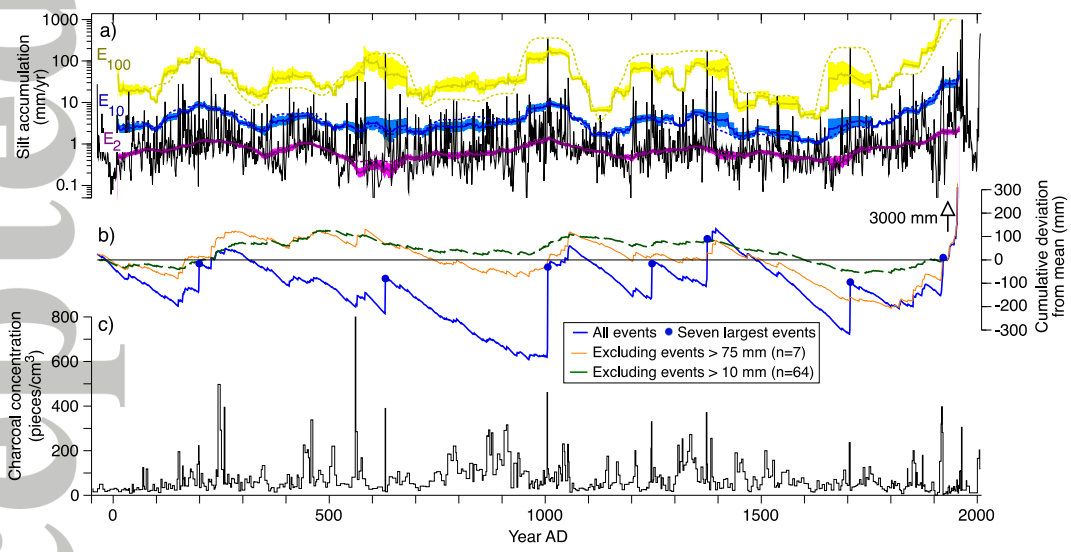

Summary figure. a) Pseudo-annual silt accumulation plotted on a log scale showing estimates of the 100-year, 10-year, and 2-year return-interval event magnitudes (E_{100}, E_{10}, and E_2, respectively) calculated in a 99-year moving window. Solid line and background shading indicate the estimated values and 95% confidence intervals from RMA regression. Thin dashed lines show a loess-smoothed quantiles within the same moving window; b) cumulative deviation of sediment accumulation from the mean for the period before AD 1930. Lines were also calculated after substituting the seven largest events and the 64 largest events with the mean values. Positive excursions occur at erosion events and descending trends correspond to the slow accumulation of sediment between events; c) charcoal concentration showing distinct peaks resulting from fire (Colombaroli and Gavin 2010).